Chapter 22

Experimental Protocols for MRI Mapping of Renal T_1

Philippe Garteiser, Octavia Bane, Sabrina Doblas, Iris Friedli, Stefanie Hectors, Gwenaël Pagé, Bernard E. Van Beers, and John C. Waterton

Abstract

The water proton longitudinal relaxation time, T_1, is a common and useful MR parameter in nephrology research. Here we provide three step-by-step T_1-mapping protocols suitable for different types of nephrology research. Firstly, we provide a single-slice 2D saturation recovery protocol suitable for studies of global pathology, where whole-kidney coverage is unnecessary. Secondly, we provide an inversion recovery type imaging protocol that may be optimized for specific kidney disease applications. Finally, we also provide imaging protocol for small animal kidney imaging in a clinical scanner.

This chapter is based upon work from the COST Action PARENCHIMA, a community-driven network funded by the European Cooperation in Science and Technology (COST) program of the European Union, which aims to improve the reproducibility and standardization of renal MRI biomarkers. This analysis protocol chapter is complemented by two separate chapters describing the basic concept and experimental procedure.

Key words Magnetic resonance imaging (MRI), Kidney, Mice, Rats, Longitudinal relaxation time (T_1), Spin-lattice relaxation time (T_1)

1 Introduction

The water proton longitudinal (or spin-lattice) relaxation time, T_1 (s), is a MR parameter commonly used in biomedical imaging. Unlike machine-dependent metrics such as "signal intensity in T_1-weighted MRI," T_1 measures a real physical process (i.e., the return to Boltzmann equilibrium of water proton longitudinal magnetisation) measured in absolute units (s) and, for any given magnetic field strength, independent of the machine used. Renal pathology often results in abnormal T_1 either globally (e.g., in renal failure) or focally (e.g., in renal cancer). Moreover, disease-induced changes in T_1 can often be assigned, at least qualitatively, to pathological changes such as fibrosis, inflammation, and oedema [1]. A second motivation to measure T_1 is in so-called dynamic experiments. In

Andreas Pohlmann and Thoralf Niendorf (eds.), *Preclinical MRI of the Kidney: Methods and Protocols*, Methods in Molecular Biology, vol. 2216, https://doi.org/10.1007/978-1-0716-0978-1_22,

this case the object under investigation in the MRI scanner for a short period (e.g., 10 min) while T_1 is measured repetitively, during some intervention to perturb T_1 (e.g., contrast agent administration). After administration of a contrast agent such as manganese, a gadolinium chelate, or dioxygen, changes in T_1 are linearly related to the contrast agent concentration, which could not reliably be determined from signal intensity changes alone.

Here we describe MRI protocols for mapping and monitoring T_1 in the kidney of small rodents in a step-by-step experimental protocol. The rationale for choosing different acquisition parameters depending to the aims of the study is discussed, together with specific parameter examples. T_1 measurements for dynamic studies are discussed in the chapter by Irrera P et al. "Dynamic Contrast Enhanced (DCE) MRI-Derived Renal Perfusion and Filtration: Experimental Protocol."

1.1 Motivation for Measuring T_1 in Animal Kidneys

Imaging provides many useful metrics in animal models of kidney physiology and pathophysiology. These include "extensive" or size variables, such as renal volume (ml) or thickness (mm) of renal cortex, and "intensive" or tissue characterisation variables, such as the longitudinal relaxation time, T_1 (s). Some investigators prefer to report the longitudinal relaxation rate R_1, the reciprocal of T_1, because from a metrology perspective R_1 is a "ratio variable" while T_1 is merely an "interval variable" [2]. In this work we use T_1. "Intensive" variables can be mapped, the maps themselves being a type of image. Such image metrics used in animal studies are valuable in translational research, as they are directly comparable with the imaging markers [3–5] used in studies of human subjects.

1.2 Study Design Concepts

Great care is needed in the choice of method to map T_1. No single method is optimal for all in vivo studies. The most accurate methods (e.g., inversion recovery with long TR and short TE readout) are neither fast nor efficient. In vivo studies involve complex trade-offs between accuracy, speed, spatial resolution, field of view, need for fat suppression, sensitivity to inflow, sensitivity to motion artifact, biexponential T_1 decay, and other confounding tissue magnetisation behaviours such as transverse relaxation and magnetisation transfer. Moreover, even after a specific method is chosen, errors can be very sensitive to pulse sequence parameters such as delays, flip angles, spoiling and refocussing strategies, mis-set RF pulses and so on. For the renal investigator the first question in designing a study to measure T_1 must always be: *what is the aim of the study?*

1. For studies of global pathology, very high spatial and temporal resolution may be unnecessary provided that the cortex, the zones of the medulla, and the papilla can be resolved. In such studies a 2D image with voxel size of around 0.25 mm (in mice, e.g., [6–8]) or around 0.5 mm (in rats, e.g., [9–12]) may be adequate. It is often desirable to acquire T_1 with low

uncertainty so that small early pathological changes can be detected, and also to acquire accurate T_1 values that are reproducible between centers so that findings are generalizable. A saturation recovery sequence with ten or more inversion times, a 2D RARE readout, moderate spatial resolution, and a two- or three-parameter fit, should provide T_1 values which are not biased by B_1^+ errors. Alternately an inversion recovery sequence with a 2D echo-planar readout [6, 8] may be used although this is less time-efficient. The accuracy of the T_1 acquisition and analysis method should be verified using phantoms of known T_1 [2].

2. Studies of focal pathology may require high spatial resolution in 3D appropriate to the disease under investigation. Low uncertainty, high accuracy, and high reproducibility are also likely to be important so that scan times may be relatively long. 3D variable flip angle sequences are convenient, although they are quite vulnerable to B_1^+ errors. In these cases, phantom studies are highly desirable to mitigate B_1^+ errors, although phantom studies do not mitigate the motion artifact error to which these sequences are also highly vulnerable.
3. Longitudinal studies, during the development and/or treatment of disease have similar demands on spatial and temporal resolution, although if the study endpoint is the change in T_1, requirements for accuracy may be relaxed: in a significance test of post vs pre, or treated vs untreated, systematic errors from biased T_1 measurement may partly cancel out.
4. Dynamic studies have similar demands on spatial resolution (e.g., high 3D resolution for focal disease) together with very good temporal resolution to allow dynamic changes to be quantitated. In consequence accuracy may be compromised, but since the study endpoint relies on T_1 change during the dynamic run, bias may partly cancel out. Propagation of errors in these cases can be exceedingly complex and requires careful simulation.

1.3 Data Quality

It is highly desirable to verify the accuracy and repeatability of T_1 using phantoms [2], before experimental animals are exposed to study procedures. The design of MR phantoms can be challenging, and while validated traceable phantoms have been developed by metrologists for clinical MR [13–15], these are usually too large for use in rodent MR scanners. Design considerations should include biological, chemical, and physical stability, temperature independence, convenience, and cost. The phantom should cover both the expected T_1 range and the spatial range, since it may be advantageous to position the kidneys offset relative to the magnet's isocenter [16]. Nickel-doped agarose gels [17–19] are particularly convenient as simple liquid flood phantoms may introduce artifacts from unfamiliar MR phenomena such as radiation damping, convection, excessive T_2 or self-diffusion, standing waves, or abrupt boundaries.

This chapter is part of the book Pohlmann A, Niendorf T (eds) (2020) Preclinical MRI of the Kidney—Methods and Protocols. Springer, New York.

2 General Considerations

2.1 Magnetic Field Strengths

Animal kidney MRI has been performed at a wide range of magnetic field strengths (B_0) between at least 0.4 T [20] and 16.4 T [21]. T_1 increases with B_0 [22]. Hence it is important to consider B_0 as an important factor in experiment design, although in practice B_0 may not be an adjustable parameter since many facilities only have a single MRI machine operated at a single magnetic field strength available. Higher magnetic field strengths are not always preferable, as the scan times required to properly sample the recovery of longitudinal magnetization will be somewhat longer, and problems from motion artifact, chemical shift artifact or susceptibility variation may increase. For an investigator who wishes to use rodent renal T_1 changes to study, say, the development of fibrosis or inflammation, the relevant metric is T_1 contrast-to-noise ratio per unit time, which does not necessarily improve as field strength increases: a high-field ($\geq$9.4 T) magnet may be no better than a conventional 3-7 T magnet. On the other hand, for an investigator who measures the uptake of a relaxive substance such as dioxygen, manganese, or gadolinium chelate, a high-field magnet provides a lower baseline R_1, making the induced changes ΔR_1 more evident.

2.2 Physiologic Motion

Acquisition parameters should ensure that interference from physiologic motion on the signal is kept to a minimum. Indeed, although kidneys are positioned quite low in the abdomen, they are still subject to mild respiratory motion artifacts. It is possible to acquire continuously under shallow breathing, taking advantage of the slow speed of breathing in anesthetized animals [23]. With such datasets, some of this motion can be corrected for during image processing with appropriate coregistration strategies or by intentionally skipping frames presenting a high degree of respiratory motion from the analysis. However, because this strategy potentially removes important datapoints or because it introduces physiological noise into the quantitative estimation, it is still recommended to implement motion compensation strategies at the acquisition level. In particular, respiratory motion compensation takes advantage of a respiratory signal (acquired externally or with MR signals such as navigators) to only allow acquisition during the long periods of breathing motion arrest that are typical of anesthetized animals. An example of such a setup applied to a clinical scanner, is depicted in Fig. 1. Special care is needed to ensure such triggering approaches are compatible with T_1 mapping protocols. In such protocols, sequence timing dictates the effective repetition time, upon which the accuracy of the T_1 computation is

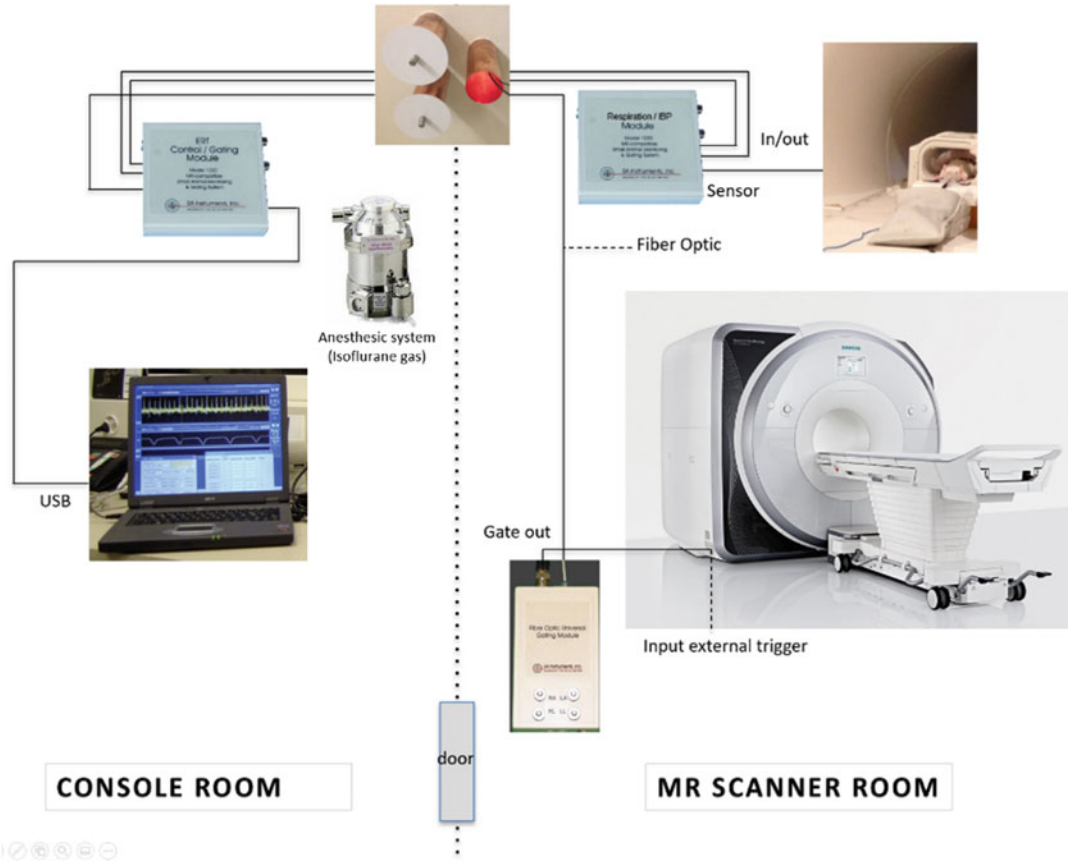

Fig. 1 Scheme of the experimental setup for a respiratory-gated implementation with monitoring small animal system SA Instruments, Inc., Stony Brook, NY11790 USA

based. It is sometimes preferred to position the trigger on the inversion (or saturation) RF pulse rather than on the slice selection or other imaging loops [16] so that the timing of image acquisition relative to inversion is guaranteed. The only timing affected in this strategy is the delay between saturation or inversion slices. In inversion recovery protocols this delay is already very long, (often more than 10 s), so any additional delay incurred will not significantly affect T_1 accuracy, while in saturation recovery the saturation pulse destroys the longitudinal magnetization so that preceding delays are unable to affect T_1 accuracy.

An alternative approach for respiratory motion compensation is retrospective gating or self-gating, which is compatible with gradient echo methods such as Variable Flip Angle (VFA). In this case, data are acquired continuously but an additional "navigator" signal allows data displaced by respiration to be sorted or discarded. This is marketed under the brand-name "IntraGate" (Bruker Biospin, Ettlingen, Germany).

Because kidneys are anatomically close to the bowels, some authors favor imaging sessions done after fasting periods [10]. Fasting should only be done after considering the physiologic

consequences, and from the animal welfare perspective should be of the minimum duration consistent with the imaging aims.

3 Imaging Techniques

Conventionally, for T_1 measurement, signal intensity is probed at different time points during exponential decay back to Boltzmann equilibrium following inversion or saturation of the longitudinal magnetization: inversion recovery or saturation recovery. Saturation can be achieved using a specific saturation pulse, or simply by varying the repetition time TR of a conventional spin echo or gradient echo acquisition which also incidentally saturates the magnetization. To reduce the total acquisition time, the Look Locker (LL) sequence can be used. With LL sequences, the magnetization is also prepared with an inversion or saturation pulse [24], but instead of a single sample of the recovery curve per TR, multiple samples are taken using a train of low flip angle pulses [25].

The inversion recovery sequence is the reference method to calculate T_1 but it suffers from long acquisition times. Therefore, the use of Look-Locker inversion recovery is advantageous, but is limited to single 2D slice acquisition: if multiple slices are needed, they must be acquired sequentially.

The alternative approach involves repeating a gradient echo acquisition at varying flip angles (VFA) while keeping TR and other sequence parameters constant: since the signal depends sinusoidally on flip angle but decays exponentially with T_1, the T_1 can be calculated from the Ernst equation (chapter by Garteiser P et al. "Analysis Protocols for MRI Mapping of Renal T_1"). Three-dimensional acquisition (3D) can be performed with VFA, but since VFA is sensitive to B_1^+ inhomogeneity, the B_1^+ field should be mapped to allow correction (chapter by Garteiser P et al. "Analysis Protocols for MRI Mapping of Renal T_1"). Although 3D VFA is familiar in clinical imaging, it is not commonly employed in rodent kidney studies, and we have not provided a protocol here.

3.1 RARE-VTR

3.1.1 Protocol Description

Rapid acquisition with relaxation enhancement at variable TR (RARE-VTR) is a type of saturation recovery sequence. Data are acquired as 2D slices, so this sequence is ideal when a single slice provides an adequate sample of the kidney, for example in the case of homogeneous global pathology. If volumetric data are required then a stack of slices must be acquired sequentially, which is time-consuming.

The RARE-VTR protocol is based on the multiecho RARE protocol, with a slice-selective 90° rf pulse followed by a train of slice-selective 180° refocusing pulses separated by an inter-echo time TE (Fig. 2). Each 180° pulse induces a refocused echo comprising spin-echo and stimulated echo contributions, which is

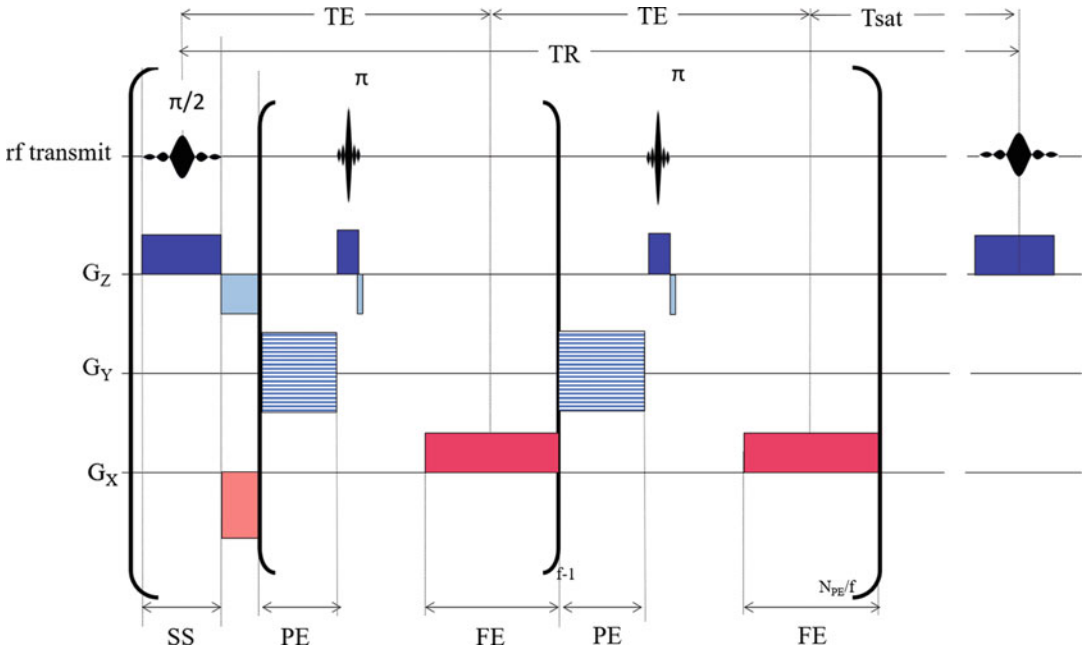

Fig. 2 Simplified timing diagram for 2D saturation recovery sequence with RARE readout. A series of 180° pulses creates *f* echoes at TE, 2 × TE, 3 × TE, and so on, where *f* is the RARE factor, typically $f = 8$. During the phase encoding (PE) step, spatial location is encoded by incrementing the *Y* gradient N_Y times so that each echo is encoded with a different phase, thereby accelerating the k-space coverage. During the frequency encoding (FE) readout periods, the spatial location is encoded in the frequency content of the digitized signal from the echo. If the pulses are perfect and if neglecting the longitudinal regrowth occurring during the echo train, all the magnetization is effectively kept in the transverse plane until the last echo (Phase cycling and spoiling not shown)

digitized, and each echo experiences a different phase encode gradient. Following the last echo there is a delay following which the sequence is repeated with a repetition time TR. The number of 180° pulses is called the echo train length (ETL) or RARE factor: a typical value is 8. TR is then varied to sample the magnetization recovery. A saturation recovery time T_{sat} is defined as TR − (ETL × TE). Thus if an investigator requires a 128^2 matrix, the entire acquisition duration would be $\Sigma TR \times 128/ETL$, where ΣTR is the sum of all the TR values used to sample the longitudinal magnetization recovery. Recommended acquisition parameters are given in section 4 below.

Because of the presence of refocusing RF pulses, this protocol is relatively insensitive to B_0 imperfections and susceptibility artifacts. For 2D single-slice T_1 mapping it is quite time-efficient, but acquisition of a multislice stack requires rather long acquisition times.

3.1.2 *Repetition Times*

The set of repetition times that are sampled needs careful consideration. The TR values should be rationally selected during preliminary studies with the animal model under investigation. In

saturation recovery experiments, the signal starts at $S_0 \sim 0$ at short TRs ($TR \ll T_1$) and increases with approximately linear S_∞/T_1 dependence on TR. At longer TRs ($TR \approx T_1$), the signal enters a transition regime where the increase in signal per unit TR diminishes. Finally at large TRs ($TR \gg T_1$), the signal asymptotically approaches S_∞. Hence, proper TR sampling strategy should be adopted to cover both regimes and the transition in between.

In determining the set of repetition times to use, the first question may be to select the highest TR that is required. This choice is mainly dictated by the expected T_1 in the tissue of interest, the available scan time and the planned postprocessing strategy.

For the first constraint, literature values or preliminary studies may help in the determination of the expected tissue T_1 at the corresponding magnetic field strength. The longest TR should be substantially larger than the longest expected tissue T_1. Typical T_1 values for cortex and medulla are in the range 1–2 s and for urine around 3 s. There is no generally accepted consensus, but authors typically have the maximal TR be 3–5 times the longest expected T_1, typically 8–12 s. If the investigator finds this makes the overall study duration too long then spatial resolution can be reduced, particularly when small focal changes are not of interest. Alternatively a maximal TR of two times the longest expected T_1 could be considered, but in this case it is recommended to perform careful simulations to ensure the propagated errors are at an acceptable level. A special case arises in contrast agent injection studies. Here, the distribution of the agent into the tissue of interest is quantified by looking at the absolute change in R_1 after vs before injection. Hence, care should be taken to consider that the T_1 value may be significantly shorter after injection. It may be necessary to adopt a different maximal TR for the pre- and postinjection scans. Contrast agents decrease T_1, hence the possible decrease in longest TR that is afforded has the additional consequence of shortening the scan duration. This is potentially advantageous, especially when the dynamics of contrast agent distribution needs to be interrogated and is slow (on the order of minutes). In this case it becomes feasible to monitor the contrast agent distribution dynamically by repetitively acquiring T_1 maps. Temporal resolutions of under 2 min can reasonably be achieved by trading off, for example, spatial resolution. This strategy is compatible with some contrast agent dynamics such as in manganese-enhanced MRI [21].

The choice of the longest TR should be done in harmony with the particular postprocessing solution that is planned. Indeed, the dataset obtained with the longest applied TR may be used to provide an estimate for the total equilibrium signal S_∞. In that case, the mathematical problem to be solved is reduced since S_∞ can be inserted in the fitting equation, thereby removing a degree of freedom and making the fit more robust. This comes at the cost

of the necessity to acquire a scan at very long TR to ensure the signal is close enough to equilibrium values. When such an estimate of S_∞ is available, it may no longer be necessary to sample other TRs longer than the tissue T_1, concentrating instead on TR values at and below the tissue T_1 [21].

Once the largest TR to acquire has been selected, the number of TRs should be determined. The set of TR values should span the range of expected T_1. Depending on the fitting equation that is used, a larger number of repetition times may be required to provide sufficient overdetermination for the fitting procedure. In other words, there should be significantly more TRs sampled than there are free parameters in the fitted equation. In an ideal situation with negligible experimental noise, it may be sufficient to select only a number of TR values equal to the number of free parameters in the fit. However, with experimental noise, this rapidly becomes insufficient and introduces bias into the results. Hence, when signal to noise ratio is limited, it is recommended to acquire a larger number of TR values. This comes at the cost of increased scan time, since each TR is generally acquired sequentially. In saturation recovery sequences, the fitting equation only has a limited number of parameters (i.e., S_∞, R_1, and maybe S_0 and/or an error term); hence, as few as four TR values are acceptable providing sufficient signal to noise is available and sampling is appropriately selected.

In disease models the pathology evolves slowly over days or weeks, the scan duration becomes less important, and it is possible to increase the number of TR values to 6, 8, or even 12, although from an ethical perspective the duration of the procedures should always be as short as possible. The choice of TR values can even be done a priori using Cramer-Rao lower-bound methodology. This technique optimizes the distribution of the sampled variable (in that case TR), for a given number of samples, an expected noise distribution and a signal model. It was used already with some success for cardiac T_1 mapping, where it was found that at constant number of acquired averages, increasing the SNR by averaging a carefully selected subset of TR values could prove beneficial relative to a set of uniformly distributed TR values [26]. A similar approach can be proposed to optimize the repetition times to use in kidney T_1 mapping.

In typical MRI scanners, the specific TR values can be set manually with a TR table having a user-specified number of TR entries. Manufacturers also often provide utilities that assist the user in prescribing the TR series. These utilities query from the user only a minimal value, a maximal value and a number of steps, or a minimal value, a number of steps and an estimate of the tissue T_1. These input values are then used to generate the series of TR values to use during the acquisition.

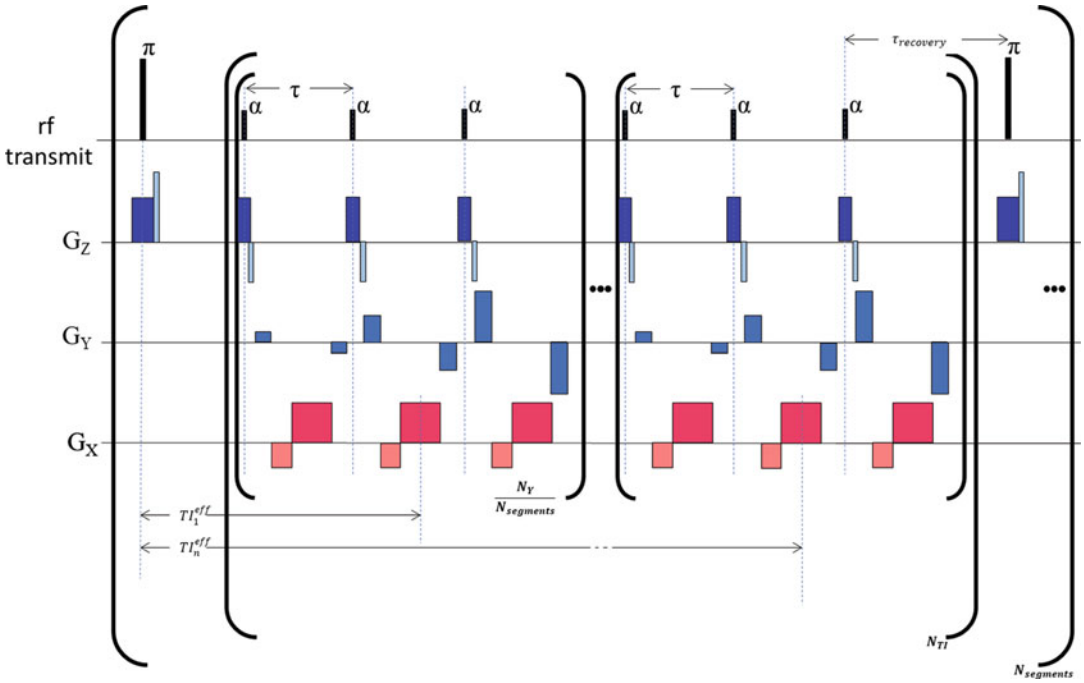

Fig. 3 Schematic view of the look-locker inversion recovery pulse sequence (fast low flip angle spoiled gradient echoes variant with spoiler gradient pulses omitted for simplicity). τ repetition time, N_y prescribed number of k-space lines, $N_{segments}$ number of k space segments (acceleration factor), *TI* inversion recovery time. Effective recovery times are considered at the centerline of each imaging segment. $\tau_{recovery}$: delay added to enable full recovery of the longitudinal magnetization before the subsequent inversion pulse is applied. In other variants, the fast low angle shots can be replaced by steady state free precession modules or EPI modules (Accessory gradient lobes are not shown for clarity)

3.2 Recovery Techniques: Look-Locker and Derivatives

3.2.1 Protocol Description

Look-Locker (LL) is a variant of inversion recovery or saturation recovery sequence. Data are acquired as 2D slices, and if volumetric data are required, a stack of slices must be acquired sequentially. LL involves sampling the magnetization using rapid, small angle imaging readouts while it recovers from the inversion or a saturation RF pulse (Fig. 3). The temporal spacing between imaging readouts provides a rapid way to sample the longitudinal regrowth. Indeed, each imaging shot will occur at a different time during regrowth, hence many different recovery times can be sampled during a single recovery event. Full longitudinal regrowth takes longer after an inversion RF pulse than after a saturation RF pulse, however, adopting an inversion RF pulse increases the dynamic range of the sampled signal. Thus the choice between saturation or inversion for the preparation of magnetization in a recovery sequence may be dictated by the experimental necessity for short acquisition time (for instance in dynamic experiments involving contrast agents with rapid kinetics) or higher measurement precision.

The Modified Look-Locker Inversion Recovery (MOLLI) sequence is an alternative when small animal renal T_1 mapping is

performed using a clinical MR system. One rationale for choosing a clinical platform for preclinical studies is the similarity between MR protocol played out on small animals and human kidneys. MOLLI was initially designed for myocardial T_1 mapping at 1.5 T [27]. A typical MOLLI sequence can be performed by acquiring single shot True FISP images at different inversion times after a single inversion pulse. MOLLI is routinely used clinically for T_1 mapping and is usually available on clinical MR systems equipped with a cardiac package. The original MOLLI sequence provided by the manufacturers' library is a good starting point for MOLLI optimization in the rodent kidney. However, translating the MOLLI technique for scanning rodent models on a clinical MR scanner requires a specific implementation. In human, MOLLI is usually acquired in breath hold. In rodent, a physiological monitoring system to track the respiration and synchronize the sequence is needed (*see* Fig. 1).

3.2.2 Types of Readouts, and Corresponding Specific Points of Attention

In recovery-type sequences, several options are possible for the imaging shots that are performed to sample the recovery period.

Fast low angle shots, where magnetization is spoiled before subsequent RF pulses, can be used. They have the advantage of a short TR (~3 ms) that is compatible with low flip angles (<10°) [9]. As such, they perturb the longitudinal regrowth of the magnetization only to a small extent.

Balanced readouts such as steady-state free precession (SSFP) can also be used, as they tend to yield higher signal to noise due to the conservation of magnetization from preceding shots [28]. The SSFP condition links the TE and TR. Because FISP involves radiofrequency phase coherence between shots, acquisition can be true-FISP, fid mode or echo mode. It acquires innermost the phase encoding (in-segments), then slices, then phase encoding (segments), then (optionally) averaging. SSFP is especially sensitive to careful shimming of the B_0. The segmenting can be performed either sequentially or by interleaving phase encode steps. The interleaved mode is recommended for inversion recovery experiments. The T_1 recovery sampling must then be setup by adjusting the time between the inversion pulse and the first imaging shot. This delay is incompressible due to the need for stabilizing the steady state condition of the magnetization. This is either done with a half flip angle pulse or with a starter (dummy) sequence, at the cost of a longer delay. Unfortunately for these reasons, the implementation of respiratory or cardiac triggering is challenging, and it is recommended to proceed by gating on the saturation or inversion pulse.

Finally, echoplanar imaging (EPI) readouts have also been proposed in that context [6, 7, 16, 29, 30]. Although they are quite advantageous due to their speed (in single shot EPI, a full k-space image may be acquired after a single excitation pulse), EPI sequences for kidney T_1 mapping are vulnerable to problems associated with EPI in general, particularly if both kidneys are to be

assessed. In particular, the EPI train is sensitive to B_0 inhomogeneity, which can become problematic at higher magnetic field strengths and in large bore systems. This effect is more important for long echo train EPIs such as single shot EPI. In this situation there is also a long effective echo time to accommodate the train length required by the single shot mode. This can be detrimental because it can increase the point spread function diameter ("smearing"), thus reducing the effective spatial resolution [30]. The long echo time of single shot EPI also comes at a disadvantage in kidneys with short T_2^* such as kidneys after injection of high concentrations of contrast agents. EPI is also associated with signal dropouts and geometric distortions at regions of strong magnetic susceptibility gradients, which sometimes occur at the kidney edges [30].

These disadvantages can be mitigated by performing segmented EPI acquisitions. In segmented EPI, full k-space acquisition is subdivided over several recovery periods, thereby enabling for decreased echo times. Segmentation will, however, increase the acquisition time, since full k-space coverage will be performed over a greater number of recovery periods. Finally, EPI image quality is also adversely affected by the presence of fat, which may be abundant in some kidney disease models such as obesity-related disease models. This can be remedied by applying fat saturation pulses [7].

3.2.3 Duration of Imaging Readouts

The duration of the imaging readouts should be short relatively to the duration of the recovery. This enables to interrogate precise inversion recovery delays rather than long intervals during which the longitudinal magnetization does vary substantially. Furthermore, short imaging readout durations are also advantageous because more imaging shots can be positioned during longitudinal regrowth. The increased number of data points yields better numerical stability during the subsequent fitting procedure.

3.2.4 Number of Imaging Readouts

The total number of imaging readouts that can be fit in a single regrowth is limited by several factors. First, the imaging sequence (excitation and readout) itself takes an incompressible minimum amount of time. Second, there is a requirement to acquire full images at each of the recovery delays. Hence, if only a single k-space line is acquired at each recovery delay, this also means that to acquire the appropriate number of k-space lines for image reconstruction (e.g., 128), an equal number of saturation or inversion recovery periods will be necessary. Since full relaxation needs to be reached (typically 10 s or more) before the next inversion RF pulse can be applied, this implies very long acquisition times (20 min or more). Hence it is important to consider acceleration schemes such as echoplanar imaging, where partial k-spaces are acquired during the regrowth rather than single k-space lines. Finally, the image acquisition readouts perturb the growing longitudinal

magnetization: the application of the imaging RF pulses slightly saturates the signal, which makes the signal regrow with a biased apparent T_1 (sometimes denoted T_1*) that is different than the true tissue T_1. This effect can be mitigated by using smaller flip angles and longer RF pulse repetition intervals. Postprocessing strategies are also available to correct for that effect (cf. the chapter by Garteiser P et al. "Analysis Protocols for MRI Mapping of Renal T_1").

3.2.5 Repetition Time

In saturation or inversion recovery type sequences, it is important to distinguish the time between RF inversion pulses and the time between imaging RF pulses. The time between saturation or inversion must take into account the T_1 of the kidney at the considered field strength. A sufficiently long recovery period must be taken into account to prevent to saturate the magnetization. Typically inversion pulses are separated by 10 s [16, 28], 18 s [6, 7] or even 20 s [30].

The repetition time between imaging segments represents the precision with which the inversion recovery will be sampled. If a high accuracy is required for the T_1, only short imaging segments with a few to a single k-space line can be adopted. This will ensure that there is only little confounding factor arising from the longitudinal regrowth occurring during each imaging segment. Conversely if a lower T_1 recovery sampling is acceptable, then imaging can be noticeably accelerated by k-space segmenting.

3.2.6 Inversion Pulses

Adiabatic passage pulses can be advantageous to ensure saturation (adiabatic half passage) or inversion (adiabatic full passage). These pulses maintain their rotation properties invariant to the B_1^+ field, provided that the pulse B_1 exceeds an adiabaticity threshold. This is of importance in the field of kidney imaging, where the presence of intraabdominal fat can be challenging for B_1 homogeneity. Hence adiabatic RF pulses such as the hyperbolic secant RF pulse, are often used in T_1-mapping protocols, as half passage for saturation recovery experiments [23, 31] or as full passage for inversion recovery experiments [16, 30]. However, these RF pulses tend to require long duration and RF power levels, which may not be compatible with all RF coils, and unless provided by the manufacturer, their frequency and phase modulation shapes may require careful design.

Generally non selective inversion RF pulses are used. Indeed, slice selective inversion RF pulses are exposed to inflow artifacts. Indeed, when a slice selective RF pulse is applied, the spins entering the imaging slice via perfusion effects, have not been resonantly exposed to the RF pulse. Hence their presence in the imaging slice will contribute to increase on average the magnetization. This effect will be higher if perfusion is elevated, and is in fact the basis for FLAIR sequences. Whenever the true tissue T_1 is the parameter

of interest, perfusion becomes a confounding factor, and inflow artifacts should be minimized. This can be achieved either by selecting an inversion slice that is significantly larger than the imaging slice to minimize the inflow artifact by creating a large region adjacent to the imaging slice that the noninverted spins need to cross before entering the imaged slice. Alternately, a nonselective saturation pulse may be adopted. In this case, even the spins that enter the imaging slice by perfusion during the imaging train are inverted, and hence they will not modify the apparent tissue T_1. Some authors recommend offsetting the position of the kidney within the radiofrequency coil to ensure that the heart is present within the effective region of the coil, to ensure maximally inverted spins throughout the entire body of the animal [16].

Recommended acquisition parameters are given in section 4 below.

3.3 Variable Flip Angle Techniques

Variable flip angle (VFA) sequences vary the flip angle of the rf excitation pulse but keep TR constant. Data can be acquired in 3D volume, so such sequences are ideal when the entire kidney must be sampled, for example in the case of heterogeneous or focal pathology (Fig. 4). However, data acquisition takes longer than for 2D sequences, and they are not robust in the presence of B_1^+ inhomogeneity.

Variable flip angle sequences are usually based on spoiled gradient echo sequences (fast low angle shot) [12, 32, 33], but the same principles can be applied with UTE sequences [34]. By virtue of their 3D nature, they are well suited for analyzing entire kidney volumes. However, the acquisition scheme where a single angle is acquired at a time also limits the number of different flip angle acquisitions that can be achieved within reasonable scanning durations. A linearization of the VFA signal provides T_1 estimates based on as little as two flip angles, although this technique is prone to noise bias. In a study at clinical field strength of 3.0 T using a wrist coil, flip angles of 5° and 26° were proposed for a rat model of acute kidney injury [12]. The use of VFA-based protocols for kidney mapping is not yet widespread at higher magnetic field strengths, but this type of sequence is applicable in other organs [34] or in tumor models [32, 33]. VFA schemes are also prone to B_1^+ field heterogeneity. Indeed, the effectively achieved flip angle at a specific location in the kidney is function of not only pulse amplitude, but also the shape and electromagnetic properties of the animal, the radiofrequency pulse design and (to a lesser extent when volume RF coils are used for RF transmission) RF coil coverage homogeneity. Thus, the B_1 field may require to be mapped first. For instance a reference T_1 map using a recovery-based sequence can be obtained and then injected into the signal equation to extract the effective flip angle [35]. Another acquisition strategy consists of measuring the B_1^+ field directly with dual angle spin echo sequence

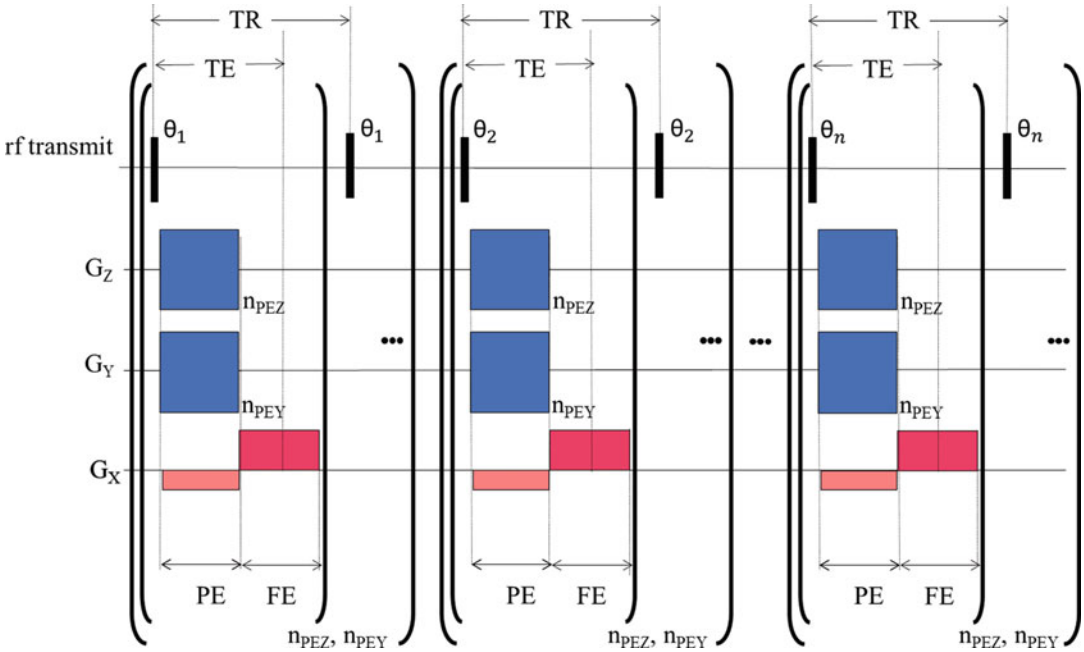

Fig. 4 3D variable flip angle protocol. *TR* repetition time (maintained constant for the duration of the acquisition), *TE* echo time, θ flip angle (flip angle is varied during the protocol), n_{PEY}, n_{PEZ} number of prescribed phase encoding lines in the *Y* and *Z* dimensions, *PE* phase encoding, *FE* frequency encoding. While the TR is maintained and constant during acquisition, the flip angle is varied several times until a complete dataset has been fully acquired for each prescribed flip angle. Accessory gradient lobes are not shown for clarity. Often, investigators need to suppress the signal from fat, in which case the hard pulse would be replaced by a spectrally selective "soft" pulse to excite ^1H_2O but not C^1H_2 or C^1H_3. During the phase-encoding (PE) step, spatial location is encoded by incrementing *X* and *Y* gradients i_X and G_Y multiple times n_{PEX} and n_{PEY}, typically 64 or 128. During this period magnetization is prephased using the *Z* gradient G_Z, so that a gradient echo may be formed by inverting the polarity of the gradient, yielding a return to phase at TE at the mid-point of the gradient echo. TE is set as short as possible, typically ~2–3 ms, in order to avoid T_2^* weighting, and to minimize total acquisition time. Practically, this is limited by the specification and performance of the gradient coils and amplifiers available to the investigator. TR is also set as short as possible, ~5 ms, in order to minimize the overall acquisition time

[36, 37]. Recommended acquisition parameters are given in section 4 below.

4 Methods

4.1 MR Protocol Setup

4.1.1 2D RARE VTR in Bruker ParaVision 6

1. Use the ParaVision RARE T1 saturation-recovery METHOD "T1map_RARE protocol" (Rat/Head/Relaxometry, or Mouse/Head/Relaxometry).
2. Set the geometry to coronal, 58 × 58 mm FOV (rat) or 40 × 30 mm FOC (mouse). These may need adjustment in studies on large (e.g., obese) animals.

3. Set the matrix size to 128 × 128; if acquisition length is too large, you may decrease the phase encoding resolution.
4. Use a single 90° 1.16 mm slice selection (optionally, apply spectrally selective fat suppression).
5. Select an180° train RARE factor 8, matching pulse bandwidths of 90° and 180°, effective TE 30 ms, echo spacing 7.5 ms.
6. Set five dummy scans; no signal averaging.
7. Set TR = 5500, 2000, 1200, 750, 500, 300, 200, and 100 ms.
8. A manufacturer-provided macro is available for data processing.

4.1.2 Inversion Recovery Sequence in Bruker ParaVision 6

1. Use the ParaVision Fluid-Attenuated Inversion Recovery (FLAIR) method using only the global inversion mode (FairMode set to Nonselective), using Flow-sensitive Alternating Inversion Recovery FAIR-RARE or FAIR-EPI Bruker methods.
2. Set the geometry to axial or coronal, 58 × 58 mm FOV (rat) or 40 × 30 mm FOV (mouse). These may need adjustment on large (e.g., obese) animals.
3. Use a single 1 mm slice selection.
4. Set the matrix size to 128 × 128 matrix; if acquisition is too long, you may diminish the spatial resolution and adopt partial Fourier acceleration.
5. Set an TE of 36 ms (FAIR-RARE) or longer (FAIR-EPI).
6. Set the inversion pulse properties to calculated, as this provides a full passage adiabatic pulse with appropriately good flip angle homogeneity.
7. Use 21 inversion times starting at 30 ms with increments of 200 ms (to be adapted to the particular study at hand).
8. Select a recovery time of 10 s or greater.
9. Adjust the number of averages based on the available scan time.
10. In case of EPI usage, a careful shimming of B0 is paramount. The manufacturer-recommended method is MapShim using an ellipsoidal shim volume, in which a B_0 map is measured (accessible in the adjustments platform) and used to correct the B_0 with the shims coils available on the system.
11. A manufacturer-provided macro is provided for data processing.

1. Install rat in a wrist coil with conventional pressure pad to monitor breath rate. Figure 1 illustrates a dedicated small animal SA Instruments system connected to a Siemens clinical MR system.

4.1.3 Modified Look-Locker Inversion Recovery (MOLLI) [27] Sequence for Rats on a Siemens Clinical Scanner

2. Load the MOLLI sequence provided by the MRI system. The original MOLLI 3(3)3(3)5 scheme can be applied for kidney imaging. In this sampling scheme, multiple images are acquired at 11 time points on the recovery curve, with three inversions with slightly shifted inversion times, enabling a pixel-based T_1 quantification.
3. Start TI at 117 ms with TI increments (ΔTI) between inversion of 80 ms.
4. The slice thickness and in-plane resolution are particularly important to avoid partial volume effects. Use a slice with the lowest thickness and the highest in-plane resolution allowed by the MR system typically resulting voxel size around $0.7 \times 1.1 \times 3.5$ mm at 3 T.
5. Set TR/TE around 711/1.09 ms.
6. Set flip angle from 28° to 35° (default flip angle of 35°) T1 map relies on kidney being aligned between all TI images. As a consequence it is important to provide an additional motion correction method to mitigate residual respiratory motion. It is recommended to perform at least a rigid registration algorithm between images from various inversion times before the pixel-wise analysis of the relaxation curve (cf. the chapter by Garteiser P et al. "Analysis Protocols for MRI Mapping of Renal T_1"). Some vendors proposed on line motion correction algorithm, such as MOCCO from Siemens, during the reconstruction process.

4.2 Calibrated Phantom Acquisitions

1. Construct or procure a set of filled nickel/agarose phantoms without air bubbles. Each phantom should use a vial appropriate for the size of the animal abdomen (e.g., 25 mm diameter $\times$ 40 mm high for a mouse or 50 mm diameter $\times$ 80 mm high for a rat). Use 2% agarose, and a different concentration of nickel chloride in each phantom. Suitable nickel concentrations are 0 mM, 0.5 M, 1 mM, 2 mM, and 4 mM: 8 mM, and 16 mM can be added if very short T_1 values are expected (e.g., in DCEMRI). Add a preservative, such as 0.05% sodium azide, and seal.
2. Measure T_1 for each phantom using the method of Subheading 4.3 and the chapter by Garteiser P et al. "Analysis Protocols for MRI Mapping of Renal T_1." Repeat the measurements on a different day. Temperature should be controlled carefully, for instance by isolating the T_1 phantom in an ice–water mixture, or by inserting the phantom in a larger structure with high thermal inertia and preequilibrated at the target temperature.
3. In consultation with a professional statistician, calculate the repeatability and ensure the sample size is adequate to test the

hypothesis of interest. From an ethical perspective, this is mandatory before living animals are entered into the procedures.

4. Repeat **steps 2** and **3** in a group of living animals. The group size should be determined in consultation with a professional statistician: group sizes of between 6 and 15 are common.

4.3 Animal Experiments (Dedicated Small Animal MR Systems)

1. Use a volume RF coil of suitable diameter. In dedicated preclinical MRI, volume RF coils with an inner diameter of 38 mm for mice or 72 mm for rats could be used.
2. Anesthetize the animal with isoflurane as described in the chapter by Kaucsar T et al. "Preparation and Monitoring of Small Animals in Renal MRI" and transfer it to the scanner.
3. Set up the temperature monitoring (rectal probe) and respiratory monitoring (balloon on chest) unit.
4. Perform anatomical imaging as described in the chapter by Pohlmann A et al. "Essential Practical Steps for MRI of the Kidney in Experimental Research."
5. Perform localized shimming on the kidney imaging as described in the chapter by Pohlmann A et al. "Essential Practical Steps for MRI of the Kidney in Experimental Research." Wherever possible, appropriate tuning and matching of the used RF coil should be done.
6. Make sure the respiratory gating is setup properly, and that the anesthesia is stable.
7. Ensure that B_1^+ is correct, that is, that the relationship between the RF power and the desired flip angle is known in the region of space occupied by the kidneys. In *ParaVision* this is performed as part of the initial sequence adjustments when the reference pulse power is calibrated.

Acknowledgments

We thank Dr. Sascha Koehler (Bruker Biospin, Ettlingen, Germany) for helpful discussions.

This chapter is based upon work from COST Action PARENCHIMA, supported by European Cooperation in Science and Technology (COST). COST (www.cost.eu) is a funding agency for research and innovation networks. COST Actions help connect research initiatives across Europe and enable scientists to enrich their ideas by sharing them with their peers. This boosts their research, career, and innovation.

PARENCHIMA (renalmri.org) is a community-driven Action in the COST program of the European Union, which unites more than 200 experts in renal MRI from 30 countries with the aim to improve the reproducibility and standardization of renal MRI biomarkers.

References

1. Friedli I, Crowe LA, Berchtold L, Moll S, Hadaya K, de Perrot T et al (2016) New magnetic resonance imaging index for renal fibrosis assessment: a comparison between diffusion-weighted imaging and T1 mapping with histological validation. Sci Rep 6:30088
2. Waterton JC, Hines CDG, Hockings PD, Laitinen I, Ziemian S, Campbell S et al (2019) Repeatability, and reproducibility of longitudinal relaxation rate in 12 small-animal MRI systems. Magn Reson Imaging 59:121–129
3. Dekkers IA, Lamb HJ (2018) Clinical application and technical considerations of T1 & T2 (*) mapping in cardiac, liver, and renal imaging. Br J Radiol 91(1092):20170825
4. Waterton JC (2013) Translational magnetic resonance imaging and spectroscopy: opportunities and challenges. In: Garrido L, Beckmann N (eds) New applications of NMR in drug discovery and development. Royal Society of Chemistry, London, pp 333–360
5. O'Connor JP, Aboagye EO, Adams JE, Aerts HJ, Barrington SF, Beer AJ et al (2017) Imaging biomarker roadmap for cancer studies. Nat Rev Clin Oncol 14(3):169–186
6. Hueper K, Peperhove M, Rong S, Gerstenberg J, Mengel M, Meier M et al (2014) T1-mapping for assessment of ischemia-induced acute kidney injury and prediction of chronic kidney disease in mice. Eur Radiol 24(9):2252–2260
7. Tewes S, Gueler F, Chen R, Gutberlet M, Jang MS, Meier M et al (2017) Functional MRI for characterization of renal perfusion impairment and edema formation due to acute kidney injury in different mouse strains. PLoS One 12(3):e0173248
8. Hueper K, Hensen B, Gutberlet M, Chen R, Hartung D, Barrmeyer A et al (2016) Kidney transplantation: multiparametric functional magnetic resonance imaging for assessment of renal allograft pathophysiology in mice. Investig Radiol 51(1):58–65
9. Kierulf-Lassen C, Nielsen PM, Qi H, Damgaard M, Laustsen C, Pedersen M et al (2017) Unilateral nephrectomy diminishes ischemic acute kidney injury through enhanced perfusion and reduced pro-inflammatory and pro-fibrotic responses. PLoS One 12(12): e0190009
10. Wang JJ, Hendrich KS, Jackson EK, Ildstad ST, Williams DS, Ho C (1998) Perfusion quantitation in transplanted rat kidney by MRI with arterial spin labeling. Kidney Int 53 (6):1783–1791
11. Ogbron MR, Sareen S, Prychitko J, Buist R, Peeling J (1997) Altered organic anion and osmolyte content and excretion in rat polycystic kidney disease: an NMR study. Am J Phys 272(1 Pt 2):F63–F69
12. Ko SF, Yip HK, Zhen YY, Lee CC, Lee CC, Huang SJ et al (2017) Severe bilateral ischemic-reperfusion renal injury: hyperacute and acute changes in apparent diffusion coefficient, T1, and T2 mapping with immunohistochemical correlations. Sci Rep 7(1):1725
13. Keenan KE, Ainslie M, Barker AJ, Boss MA, Cecil KM, Charles C et al (2018) Quantitative magnetic resonance imaging phantoms: a review and the need for a system phantom. Magn Reson Med 79(1):48–61
14. Captur G, Gatehouse P, Keenan KE, Heslinga FG, Bruehl R, Prothmann M et al (2016) A medical device-grade T1 and ECV phantom for global T1 mapping quality assurance-the T1 mapping and ECV standardization in cardiovascular magnetic resonance (T1MES) program. J Cardiovasc Magn Reson 18(1):58
15. Lerski RA, McRobbie DW, Straughan K, Walker PM, de Certaines JD, Bernard AM (1988) Multi-center trial with protocols and prototype test objects for the assessment of MRI equipment. EEC Concerted Research Project. Magn Reson Imaging 6(2):201–214
16. Rajendran R, Lew SK, Yong CX, Tan J, Wang DJ, Chuang KH (2013) Quantitative mouse renal perfusion using arterial spin labeling. NMR Biomed 26(10):1225–1232
17. Christoffersson JO, Olsson LE, Sjoberg S (1991) Nickel-doped agarose gel phantoms in MR imaging. Acta Radiol 32(5):426–431
18. Kraft KA, Fatouros PP, Clarke GD, Kishore PR (1987) An MRI phantom material for quantitative relaxometry. Magn Reson Med 5 (6):555–562
19. Howe FA (1988) Relaxation times in paramagnetically doped agarose gels as a function of temperature and ion concentration. Magn Reson Imaging 6(3):263–270
20. Finney JS, Bach PH, Bushell MC, Gregg NM, Taylor DG (1990) The application of proton nuclear magnetic resonance imaging for the in vivo characterisation of chemically induced renal lesions in rats over a prolonged time study. Magn Reson Imaging 8(6):713–721
21. Jiang K, Tang H, Mishra PK, Macura SI, Lerman LO (2018) A rapid T1 mapping method for assessment of murine kidney viability using

dynamic manganese-enhanced magnetic resonance imaging. Magn Reson Med 80 (1):190–199
22. Korb JP, Bryant RG (2002) Magnetic field dependence of proton spin-lattice relaxation times. Magn Reson Med 48(1):21–26
23. Zhang J, Chamberlain R, Etheridge M, Idiyatullin D, Corum C, Bischof J et al (2014) Quantifying iron-oxide nanoparticles at high concentration based on longitudinal relaxation using a three-dimensional SWIFT Look-Locker sequence. Magn Reson Med 71 (6):1982–1988
24. Chow K, Flewitt JA, Green JD, Pagano JJ, Friedrich MG, Thompson RB (2014) Saturation recovery single-shot acquisition (SASHA) for myocardial T(1) mapping. Magn Reson Med 71(6):2082–2095
25. Stikov N, Boudreau M, Levesque IR, Tardif CL, Barral JK, Pike GB (2015) On the accuracy of T1 mapping: searching for common ground. Magn Reson Med 73(2):514–522
26. Akcakaya M, Weingartner S, Roujol S, Nezafat R (2015) On the selection of sampling points for myocardial T1 mapping. Magn Reson Med 73(5):1741–1753
27. Messroghli DR, Radjenovic A, Kozerke S, Higgins DM, Sivananthan MU, Ridgway JP (2004) Modified Look-Locker inversion recovery (MOLLI) for high-resolution T1 mapping of the heart. Magn Reson Med 52(1):141–146
28. Little RA, Jamin Y, Boult JKR, Naish JH, Watson Y, Cheung S et al (2018) Mapping hypoxia in renal carcinoma with oxygen-enhanced MRI: comparison with intrinsic susceptibility MRI and pathology. Radiology 288 (3):739–747
29. Hueper K, Gutberlet M, Rong S, Hartung D, Mengel M, Lu X et al (2014) Acute kidney injury: arterial spin labeling to monitor renal perfusion impairment in mice-comparison with histopathologic results and renal function. Radiology 270(1):117–124
30. Pastor G, Jimenez-Gonzalez M, Plaza-Garcia S, Beraza M, Reese T (2017) Fast T1 and T2 mapping methods: the zoomed U-FLARE sequence compared with EPI and snapshot-FLASH for abdominal imaging at 11.7 Tesla. MAGMA 30(3):299–307
31. Zhang J, Ring HL, Hurley KR, Shao Q, Carlson CS, Idiyatullin D et al (2017) Quantification and biodistribution of iron oxide nanoparticles in the primary clearance organs of mice using T1 contrast for heating. Magn Reson Med 78(2):702–712
32. Subashi E, Choudhury KR, Johnson GA (2014) An analysis of the uncertainty and bias in DCE-MRI measurements using the spoiled gradient-recalled echo pulse sequence. Med Phys 41(3):032301
33. Vautier J, Heilmann M, Walczak C, Mispelter J, Volk A (2010) 2D and 3D radial multi-gradient-echo DCE MRI in murine tumor models with dynamic R*2-corrected R1 mapping. Magn Reson Med 64(1):313–318
34. Alamidi DF, Smailagic A, Bidar AW, Parker NS, Olsson M, Hockings PD et al (2018) Variable flip angle 3D ultrashort echo time (UTE) T1 mapping of mouse lung: a repeatability assessment. J Magn Reson Imaging. https://doi.org/10.1002/jmri.25999
35. Marques JP, Kober T, Krueger G, van der Zwaag W, Van de Moortele PF, Gruetter R (2010) MP2RAGE, a self bias-field corrected sequence for improved segmentation and T1-mapping at high field. NeuroImage 49 (2):1271–1281
36. Yoon JH, Lee JM, Kim E, Okuaki T, Han JK (2017) Quantitative liver function analysis: volumetric T1 mapping with fast multisection B1 inhomogeneity correction in hepatocyte-specific contrast-enhanced liver MR imaging. Radiology 282(2):408–417
37. Stollberger R, Wach P (1996) Imaging of the active B1 field in vivo. Magn Reson Med 35 (2):246–251